ACS APPLIED MATERIALS & INTERFACES

Research Article

Cite This: ACS Appl. Mater. Interfaces XXXX, XXX, XXX−XXX

www.acsami.org

Bone-Inspired Mineralization with Highly Aligned Cellulose Nanofibers as Template

Zheng Cheng,[†] Zhou Ye,[‡] Avi Natan,[†] Yi Ma,[†] Hongyan Li,[†] Yong Chen,[†] Liqiang Wan,[†] Conrado Aparicio,*[,‡] and Hongli Zhu*[,†]

[†]Department of Mechanical and Industrial Engineering, Northeastern University, Boston, Massachusetts 02115, United States

[‡]MDRCBB-Minnesota Dental Research Center for Biomaterials and Biomechanics, University of Minnesota, Minneapolis, Minnesota 55455, United States

Supporting Information

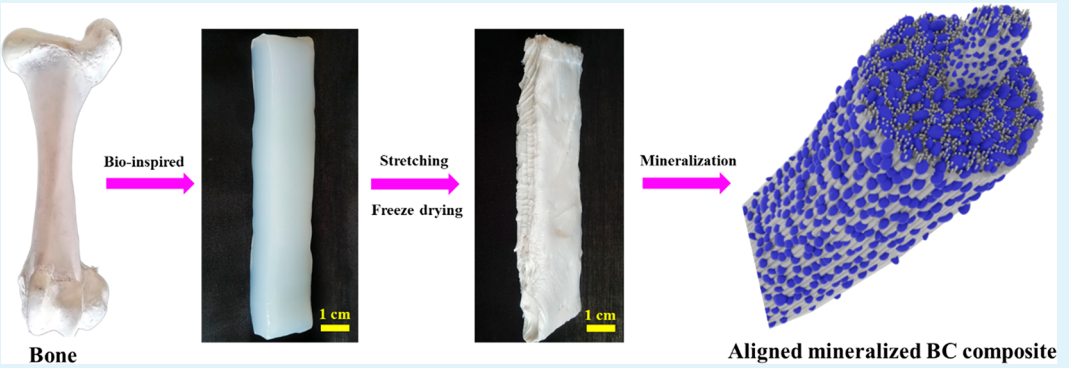

ABSTRACT: Bioinspired by the aligned structure and building blocks of bone, this work mineralized the aligned bacterial cellulose (BC) through in situ mineralization using $CaCl_2$ and K_2HPO_4 solutions. The cellulose nanofibers were aligned by a scalable stretching process. The aligned and mineralized bacterial cellulose (AMBC) homogeneously incorporated hydroxyapatite (HAP) with a high mineral content and exhibited excellent mechanical strength. The ordered 3D structure allowed the AMBC composite to achieve a high elastic modulus and hardness and the development of a nanostructure inspired by natural bone. The AMBC composite exhibited an elastic modulus of 10.91 ± 3.26 GPa and hardness of 0.37 ± 0.18 GPa. Compared with the nonaligned mineralized bacterial cellulose (NMBC) composite with mineralized crystals of HAP randomly distributed into the BC scaffolds, the AMBC composite possessed a 210% higher elastic modulus and 95% higher hardness. The obtained AMBC composite had excellent mechanical properties by mimicking the natural structure of bone, which indicated that the organic BC aerogel with aligned nanofibers was a promising template for biomimetic mineralization.

KEYWORDS: *biomimetic mineralization, alignment, hydroxyapatite composite, bacterial nanocellulose, hardness*

INTRODUCTION

The magnificent animal diversity humans enjoy today is likely a result of biomineralization. Natural hard materials like bone, teeth, and seashell are nanocomposites of organics and minerals with superior mechanical performance.[1−3] Specifically, bone is a hierarchically structured composite material primarily composed of an organic matrix (mainly collagen fibril) and an inorganic mineral phase (hydroxyapatite, HAP), which has attracted increasing interest in three bio (bioinspired, biofabrication, and biomaterial) fields.[4,5] Previous reports have indicated that crystal growth was guided by the organic matrix, which acted as a template, and the aligned organic phase improved the mechanical performance of the mineralized composite.[6] Although efforts have been made to exploit synthetic bone substitutes,[7] attempts at biomimetic mineralization of an alternative aligned organic nanofiber matrix have been scarce. Conventional methods to synthesize HAP minerals on collagen matrices have been unable to mimic the specific organic/inorganic aligned structure in bone, which give rise to either weak mechanical strength or low mineral content.[8] Hence, the development of biomimetic materials that resemble natural bone in alignment, excellent load-bearing ability, and biocompatibility is significant, but it is still a challenge because it involves the integration of two distinct phases, and it is difficult to align the organic phase.

Bacterial cellulose (BC) exhibits many superior physicochemical properties, including high purity, high crystallinity, a nanofibrillar reticulated structure, a soft elastomeric nature, high water holding capacity, and good biocompatibility.[9] Meanwhile, BC can be biosynthesized on a large scale by a fermentation process via certain bacterial species.[10] Thus BC is an attractive organic biomaterial for broad applications in the

Received: August 24, 2019
Accepted: October 22, 2019
Published: October 22, 2019

DOI: 10.1021/acsami.9b15234
ACS Appl. Mater. Interfaces XXXX, XXX, XXX−XXX

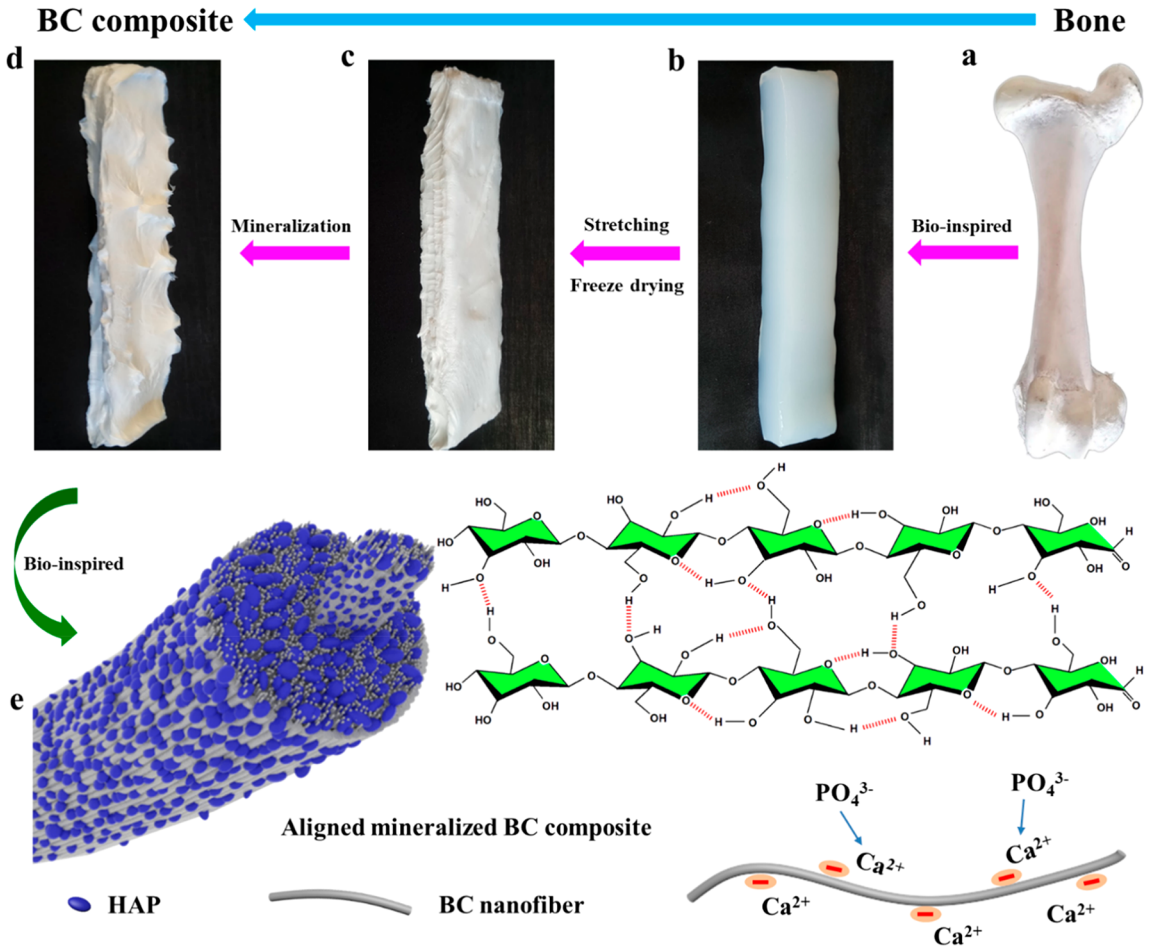

Figure 1. Schematic illustration of the mineralization process. (a) Natural bone. (b) BC hydrogel. (c) BC aerogel. (d) Mineralized BC composite. (e) Microstructure of the AMBC composite. Formation of the HAP mineral particles along the surface of aligned organic BC nanofibers.

food industry, energy storage, biomaterial fields, and so on.[11] In particular, BC has found many potential applications in the biomedical field for tissue engineering materials due to its good biocompatibility.[12] BC's mechanical properties are also similar to those of hard and soft tissues and can be easily fabricated into a variety of shapes with adjustable hierarchical pores.[13] Compared with other natural biodegradable polymers like collagen, fibrin, and chitosan, BC possesses much higher mechanical properties, which are required in most cases when used as a tissue engineering scaffold.[14] On the basis of the aforementioned advantages, the BC hydrogel has been used in biomedical fields such as wound dressings, artificial skin and blood vessels, and antimicrobial materials.[15] However, the BC aerogel with aligned nanofibers has not yet been directly used as the scaffolding biomaterial for bone tissue engineering.

It is desirable to search for a new generation of bone substitutes that not only have good mechanical properties but also are biodegradable. In recent decades, composites consisting of mineralized fibrils and calcium phosphate minerals have received much attention because they mimic the basic constituents of bone.[16] Despite their promising bioactivity, the fibrils/calcium phosphate composites have shown limited mechanical strength and are consequently challenged when it comes to practical applications. Several attempts have also been made to mineralize cellulose. In our recent publication, we used the wood-derived cellulose nanofibrils (CNFs) as the organic matrix for the biomimetic mineralization.[17] Although the mechanical properties of the resultant hybrid material was good, the CNF extraction process was typically associated with high energy and water consumption,[18] and the chemicals used to prepare CNF were costly. In addition, the mineralization process is time-consuming. Several other research experiments have also been carried out for cellulose mineralization; however, the minerals were deposited mainly on the surface and not throughout the cellulose matrix.[19,20] Meanwhile, the cellulose matrix was randomly distributed with no orientation. BC has a 3D network with finer fibers, which permits a high density of inter- and intrafibrillar hydrogen bonds.[21] Hydrogen bonding not only enables the BC to hold water in its interstitial spaces but also grants the composite high strength.

In this study, bioinspired by natural bone, the novel composite material consisting of HAP mineral crystals biomimetically deposited in the organic BC aerogel with aligned nanofibers was synthesized. The aligned organic BC nanofiber is an ideal biomaterial for biomimetic mineralization due to its orderly arrangement of nanofibers, porous structure, biocompatibility, and biodegradability. The objective of this study is to initiate biomimetic apatite formation from mineralization on the aligned BC nanofibers. The obtained aligned and mineralized bacterial cellulose (AMBC) composite exhibits a high elastic modulus and hardness of 10.91 ± 3.26 GPa and 0.37 ± 0.18 GPa, respectively, which are comparable to those of mouse trabecular bone and to the best mineralized

DOI: 10.1021/acsami.9b15234
ACS Appl. Mater. Interfaces XXXX, XXX, XXX−XXX

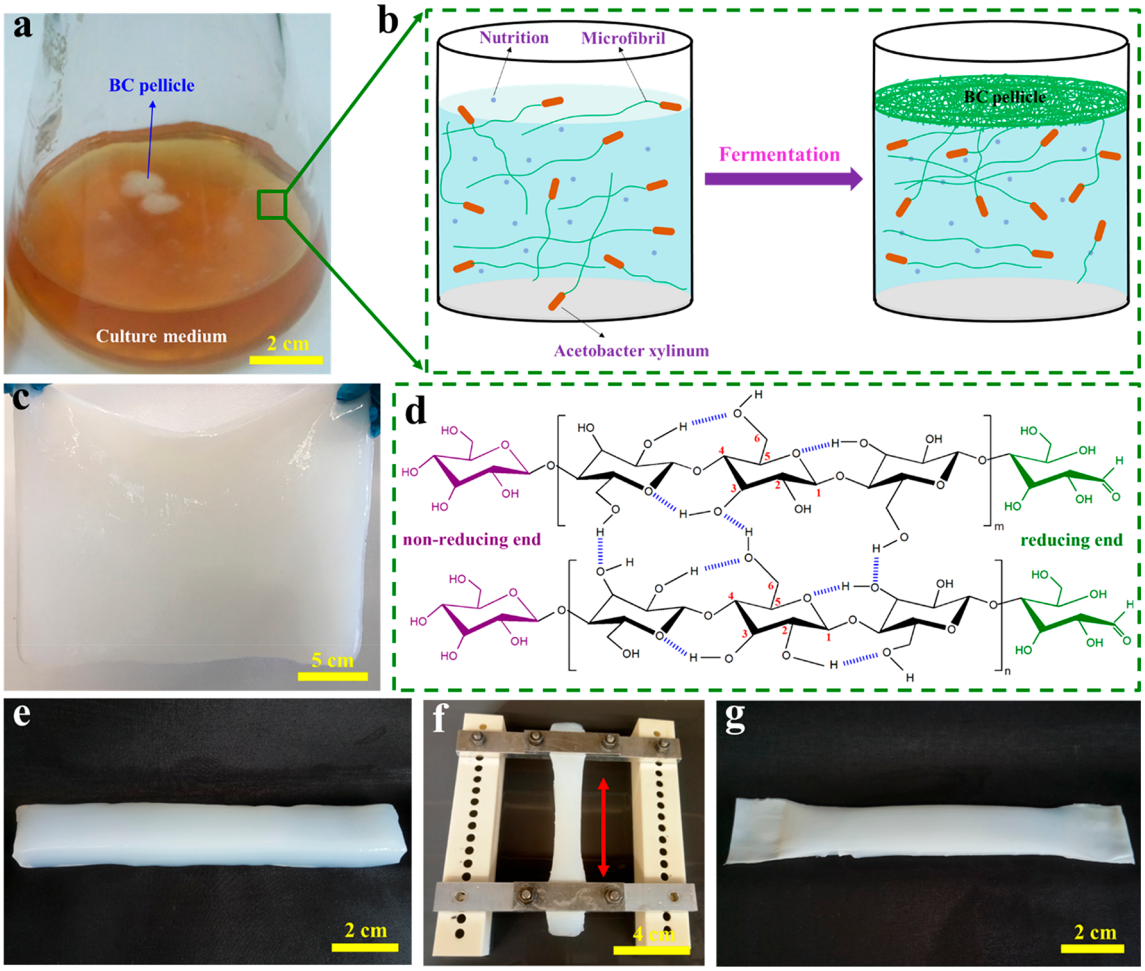

Figure 2. (a) BC pellicle is obtained via a fermentation process by *Acetobacter xylinum* under static cultivation condition. (b) Schematic illustration shows that BC nanofibers are biosynthesized in culture media containing nutrients. The BC pellicle is formed on the upper surface of liquid media. (c) Photograph of a large piece of purified BC hydrogel with water content of ~99.5% (*m*/*m*), which can be produced on a large scale. (d) Chemical structure of BC. (e) Rectangular-shaped BC hydrogel with dimensions of 120 cm × 3 cm × 20 cm (length × width × height). (f) Photograph of the BC hydrogel stretching process. The original BC hydrogel is fixed between two grips and then moved up and down at a constant speed until the stretch of the BC hydrogel reaches 20%. (g) Photograph of the stretched BC hydrogel.

organic biomass materials previously reported.[8,17] Meanwhile, a high mineral content of as much as 89.53 wt % for the AMBC composite is achieved. This aligned two-phase structure has the following advantages: (i) the homogeneous formation of HAP crystals throughout the aligned BC nanofiber host, which leads to the construction of the aligned organic BC matrix and inorganic HAP minerals, (ii) the increased hydrogen bonding between the highly aligned organic BC nanofibrils during the stretching process, and (iii) a higher HAP mineral content on aligned BC nanofibers, which benefits from the porous and high specific surface area of the BC aerogel. The aligned organic BC nanofiber mineralization in this study is more time-efficient, cost-effective, affordable, and sustainable compared with our previous study using CNF for biomineralization.[17] The AMBC is inspiring as a new class of biomaterials with high mechanical performance, potentially good osteoconductivity, as well as excellent biodegradability for bone engineering.

RESULTS AND DISCUSSION

Inspired by the aligned microstructure and basic constituents of natural bone (Figure 1a), the AMBC composite was artificially fabricated with a similar aligned structure and similar basic building blocks as bone. Figure 1 illustrates the mineralization process of organic BC aerogel and the proposed mechanism responsible for the unique structure and good mechanical properties. The aligned BC hydrogel membrane was obtained by mechanical stretching of the original BC hydrogel (Figure 1b). Next, the hydrogel was freeze-dried to obtain the BC aerogel with aligned nanofibers (Figure 1c). The AMBC composite was obtained via the alternating impregnation cycles with $CaCl_2$ and K_2HPO_4 solutions assisted by sonication and freeze-drying (Figure 1d). The structure of the obtained AMBC composite is illustrated in Figure 1e. The mechanisms for forming HAP crystals are proposed as follows: Abundant negatively charged hydroxyl groups (−OH) on the surface of BC nanofibers strongly absorb Ca^{2+} cations by an electrostatic interaction, and some Ca^{2+} ions are also trapped between the organic BC nanofibers. Thus the accumulation of Ca^{2+} ions can act as the nucleation sites and react with phosphate anions for the deposition and growth of Ca−P minerals. As a result, the organic BC aerogel with aligned nanofibers provides a fine-tuned structure for the ordered formation of HAP particles.

DOI: 10.1021/acsami.9b15234
ACS Appl. Mater. Interfaces XXXX, XXX, XXX−XXX

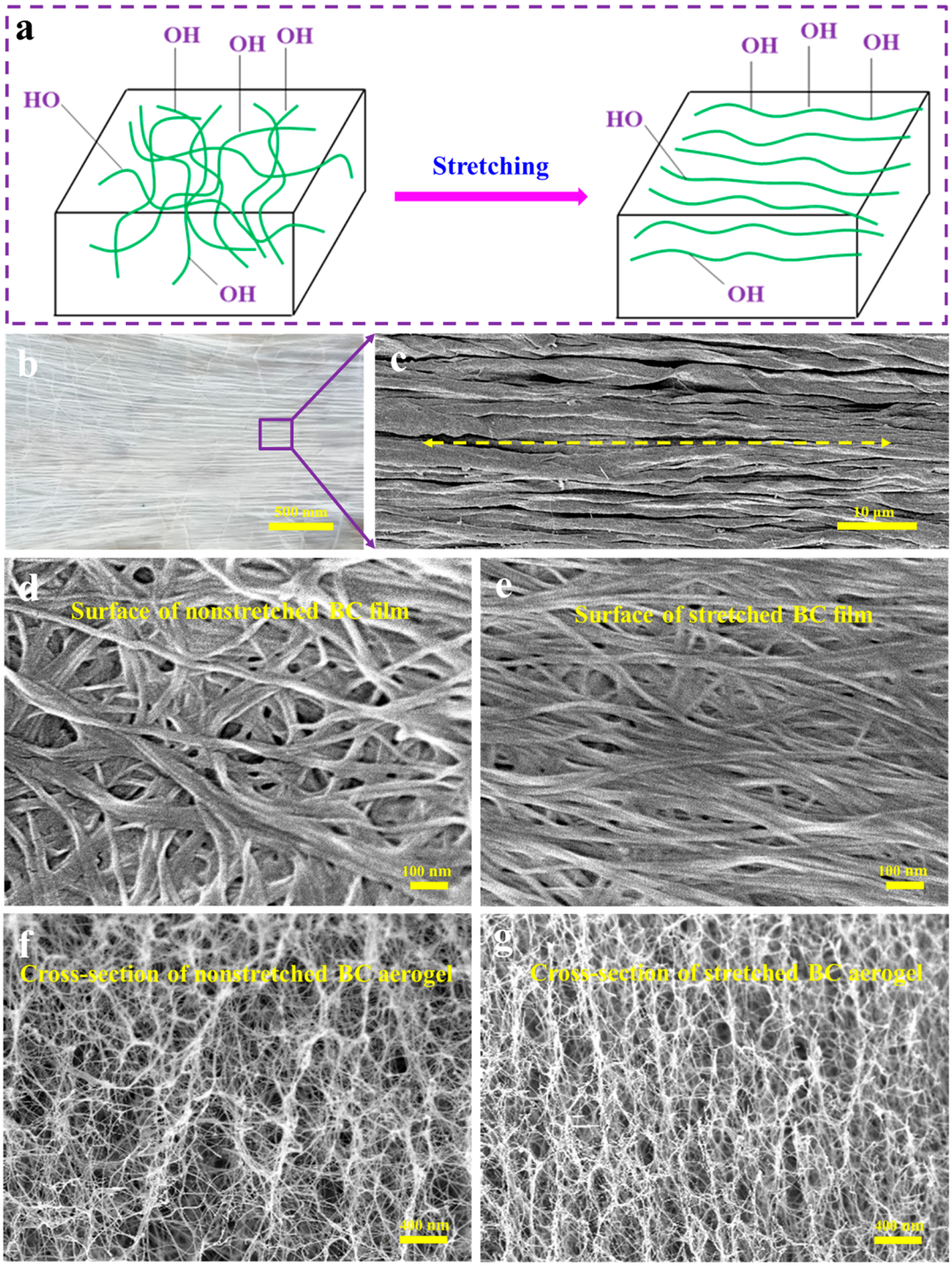

Figure 3. (a) Schematic diagram showing an increased degree of BC nanofibril orientation in the stretching direction. The nanofiber surface is negatively charged due to the high concentration of hydroxyl groups. (b) Photograph of the surface of BC film after stretching, showing its aligned pattern. (c) SEM image of the surface of the stretched film, which exhibits well-aligned microfiber bundles. SEM image of the surface morphology of BC nanofibers (d) without and (e) with stretching. SEM image of the cross-section of BC aerogel via a freeze-drying process from (f) nonstretched and (g) stretched BC hydrogel.

BC is abundant, and the mineralization process used here toward obtaining the HAP@BC strong composite is facile and scalable. The BC was biosynthesized by *Acetobacter xylinum* in culture medium under static cultivation conditions, and the BC pellicle formed on the upper surface of liquid media (Figure 2a,b). The as-prepared BC pellicles were purified by alkali solution and deionized water; then, the large piece of BC hydrogel was obtained (Figure 2c). As shown in Figure 2d, BC nanofibrils are composed of a cellulose molecule, which is a linear chain of ringed glucose molecules with the repeated unit comprising two anhydroglucose rings ($C_6H_{10}O_5$) linked through a C−O−C covalent bond. Rich hydroxyl groups in cellulose molecules enable the formation of intrachain and interchain hydrogen bonds. Therefore, the chains are firmly held together side-by-side with high tensile strength. It has been demonstrated that the structure with well-aligned

DOI: 10.1021/acsami.9b15234
ACS Appl. Mater. Interfaces XXXX, XXX, XXX−XXX

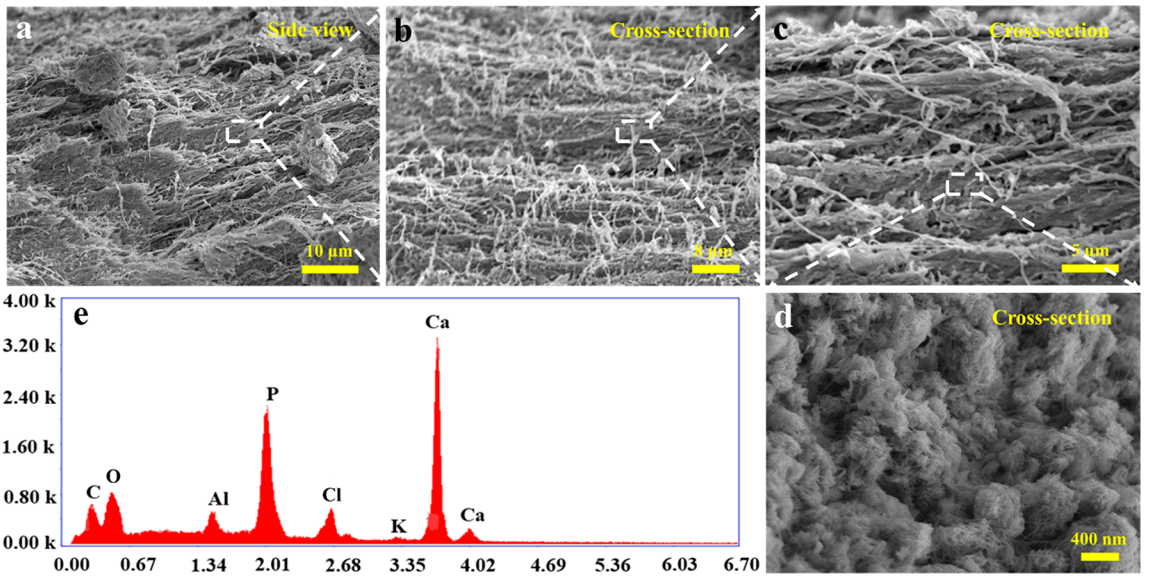

Figure 4. (a) Side view of the AMBC composite, showing the alignment of mineral nanocrystals to the orientation of nanofibers. (b) Low-magnification SEM image of the cross-section of the AMBC composite. (c) Medium-magnification SEM image of the cross-section of the AMBC composite, showing HAP mineral particles entangled with aligned organic BC nanofibers. (d) High-magnification SEM image of the cross-section of the AMBC composite, showing microstructured HAP crystals. (e) EDX of the AMBC composite from panel d.

cellulose nanofibers is important for achieving better mechanical properties.[22] In our work, a rectangular-shaped BC hydrogel of size 120 cm × 3 cm × 20 cm was obtained by cutting (Figure 2e). In the stretching process, the original BC hydrogel was fixed between two grips (Figure 2f) and then moved up and down at a constant speed until the stretch of the sample reached 20% to obtain the stretched BC hydrogel (Figure 2g). The wide BC strip became narrower and longer after stretching, which was an important step for aligning the BC nanofibers.

Herein an ultralong organic BC with aligned nanofibers via a simple and scalable wet-stretching method is reported, as illustrated in Figure 3a. The surface of BC nanofibers is negatively charged due to the existence of a large number of hydroxyl groups.[23] These groups are able to bind the Ca^{2+} ions through an ionic−dipolar interaction; then, phosphate groups become electrostatically attracted to the Ca^{2+} cations concentrated on the BC nanofibers, and the Ca−PO_4 clusters transform to HAP crystals that grow embedded in the bundles of the nanofibers. The bundles of BC fibers are clearly visible and show a well-aligned structure in the film after stretching (Figure 3b). The scanning electron microscopy (SEM) image of stretched BC film surface clearly shows that individual BC nanofibrils become densely packed to form nanofiber bundles and are aligned parallel to the stretching direction. This leads to the disappearance of the original random network structure (Figure 3c). The formation of microfiber alignment is due to the increased amount of hydrogen bonding between the highly aligned nanofibrils during the wet-stretching process. The original BC film contains randomly distributed nanofibrils with a diameter of around 30−80 nm (Figure 3d), which is the typical size of bundled elementary fibrils. The wet-stretched BC film (Figure 3e) shows an increasing amount of aligned BC nanofibrils in the orientation along the stretching direction. The BC aerogel was obtained via a simple freeze-drying process. The SEM image of the cross-section of BC aerogel clearly shows that both nonstretched and stretched BC aerogels are highly porous, which is good for the ion immersion and the eventual formation and accommodation of the HAP minerals inside the fibrillary structure. In addition, the stretched BC aerogel has better nanofiber alignment as well as a slightly reduced pore size.

BC hydrogel is an extremely soft biomaterial, which can be easily transformed into a variety of shapes. To demonstrate the excellent flexibility of the as-prepared BC hydrogel, samples are made into different shapes (Figure S1). The soft and stiff BC hydrogel can completely recover its original shape after twisting, stretching, bending, and folding in arbitrary directions without any fracture. Interestingly, the tough and strong AMBC composite is obtained after the mineralization process (Figure S2). The AMBC composite features the thorough infiltration of mineral nanocrystals distributed with the aligned organic BC nanofibers (Figure 4a). The thorough infiltration of the minerals was further confirmed by the SEM cross-sectional view (Figure 4b). A medium-magnification SEM image of the cross-section of the AMBC composite shows HAP particles entangled with aligned organic BC nanofibers (Figure 4c). In a high-magnification SEM image (Figure 4d), it is observed that several hundred microns of HAP clusters have formed within the cellulose fibrils. The BC nanofiber surface and the spaces among the fibers are fully covered with HAP clusters. The HAP particles are composed of discrete crystallites with plate-like morphology. This suggests the homogeneous formation of HAP particles throughout the BC host. Instead, the HAP crystals formed on the surface of network-structured BC nanofibers of the nonaligned mineralized bacterial cellulose (NMBC) composite (Figure S3) and did not fully infiltrate the spaces between the nanofibers. The BC aerogel with aligned nanofibers is a suitable organic substrate for ordered apatite formation. The BC aerogel is highly porous and allows ions to freely enter into the organic matrix. In addition, the pores or tunnels between the fibrils of the aligned BC aerogel matrix are relatively small, which can confine the growth of the HAP crystals, so that thorough mineralization is obtained, and thus the increase in the mechanical properties of the mineralized composite is

DOI: 10.1021/acsami.9b15234
ACS Appl. Mater. Interfaces XXXX, XXX, XXX−XXX

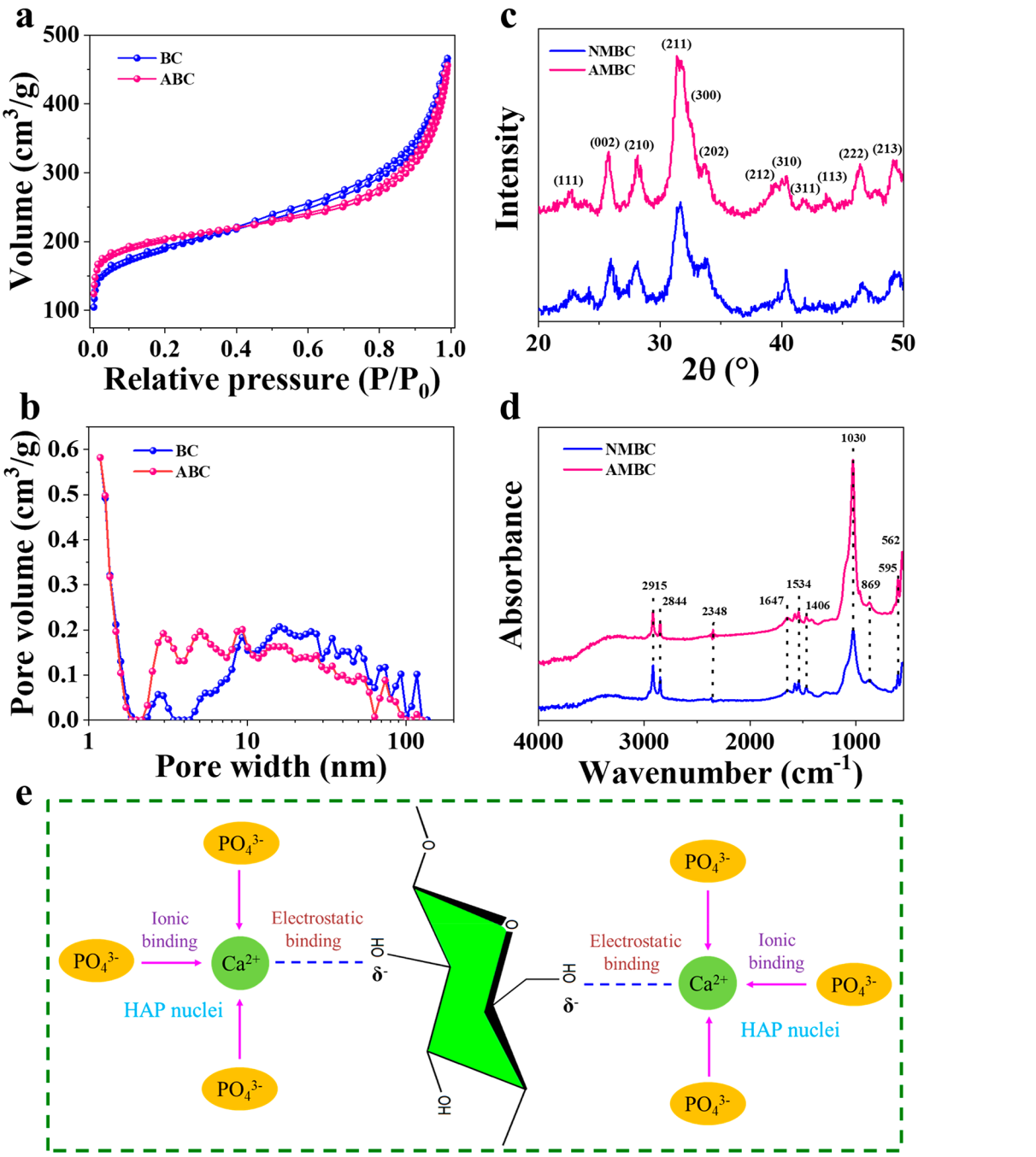

Figure 5. (a) Representative N_2 adsorption−desorption isotherm curves of BC and ABC aerogel. (b) Pore-size distributions of the BC and ABC aerogel. (c) XRD patterns of NMBC and AMBC composites. (d) FTIR spectra of NMBC and AMBC composites. (e) Detailed mechanism of the BC nanofibers interaction with calcium and phosphate ions.

expected. Lastly, the highly aligned BC nanofibers have guided and restricted the apatite growth of the discrete HAP minerals. Similar nanoconstructions exist in natural organic−inorganic hybrid composites with unique hierarchical structure, like bone and dentin.[24] The highly ordered structure of interfibrillar mineralization on the nanoscale is considered the foundation of the biomechanical properties of these naturally hard tissues.[25,26] The energy-dispersive X-ray (EDX) spectrum showed that the main components of the obtained crystals were Ca and P (Figure 4e). Furthermore, the Ca and P elements uniformly distributed throughout the fiber with a molar Ca/P ratio of 1.52. This ratio is lower than the value of stoichiometric HAP (1.67) but close to that of calcium-deficient, naturally occurring HAP.[27] In nature, the crystal lattice of calcium-deficient HAP includes small amounts of ions such as sodium (Na^+), potassium (K^+), magnesium (Mg^{2+}), and carbonate (CO_3^{2-}) as well as OH^- deficiencies and imperfections.[28] The addition or absorption of species in our mineralizing solution or the experimental environment, such as K^+ and CO_3^{2-}, can be present in the lattice structure of the obtained calcium-deficient HAP.

To assess the porosity and pore-size distribution of the BC aerogel before mineralization, the N_2 adsorption−desorption isotherm was measured. The Brunauer−Emmett−Teller

DOI: 10.1021/acsami.9b15234
ACS Appl. Mater. Interfaces XXXX, XXX, XXX−XXX

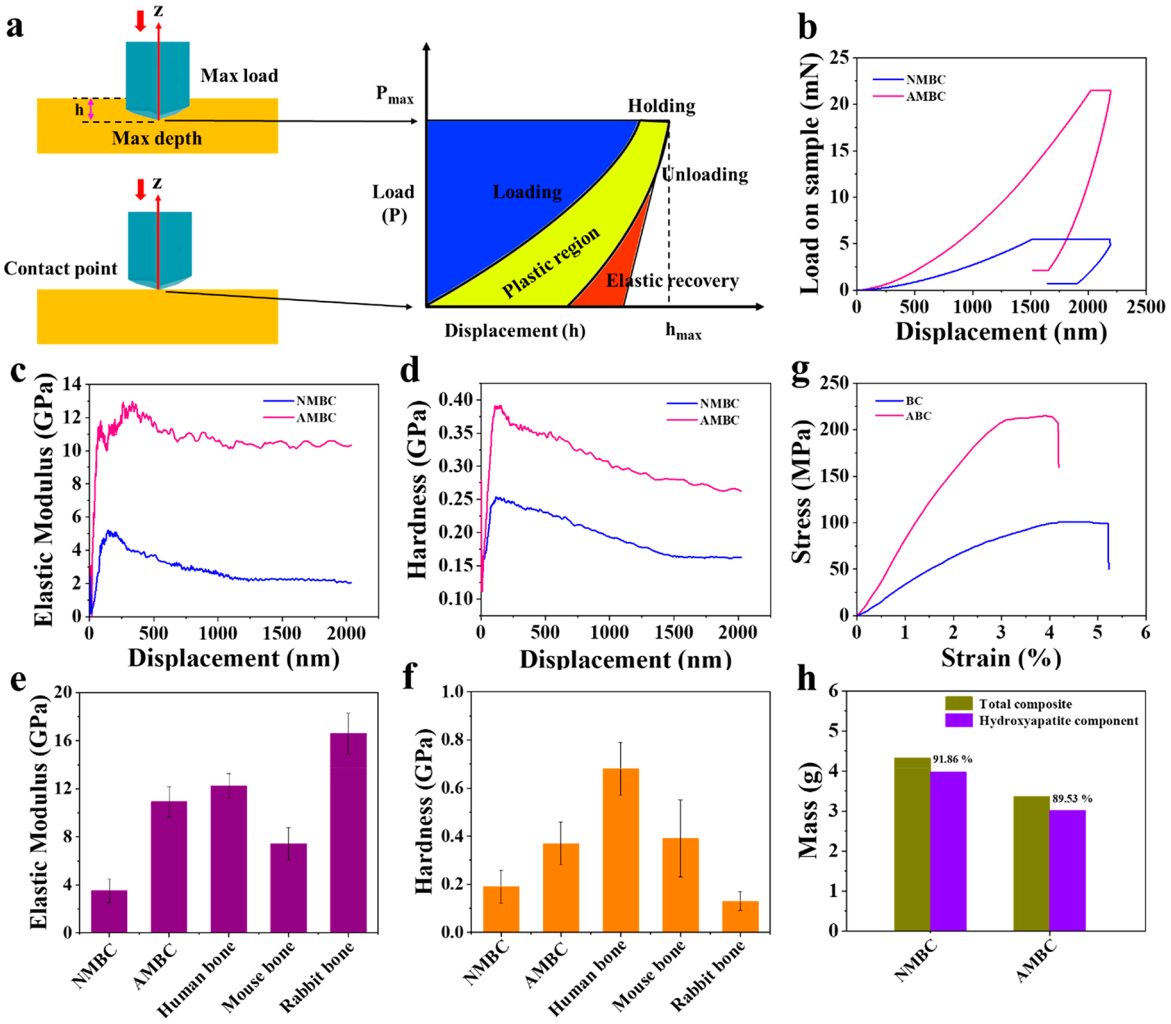

Figure 6. Mechanical tests of mineralized BC composites and BC films. (a) Schematic illustration of the nanoindentation test process and the nanoindentation graph with displacement on the horizontal axis and load on the vertical axis. (b) Representative nanoindentation load–displacement curves of the NMBC and AMBC composites. (c) Elastic modulus of NMBC and AMBC composites versus the penetration depth of the indenter. (d) Hardness of NMBC and AMBC composites versus displacement. (e) Comparison of elastic modulus on the NMBC composite, the AMBC composite, human trabecular bone,[38] mouse trabecular bone,[39] and rabbit trabecular bone[40] samples under dry conditions. (f) Comparison of hardness on the NMBC composite, the AMBC composite, human trabecular bone, mouse trabecular bone, and rabbit trabecular bone samples under dry conditions. (g) Stress–strain behavior of the BC and ABC film. (h) Mass of the total HAP@BC composites and hydroxyapatite components in NMBC and AMBC composites.

(BET) analysis of the data of the stretched BC aerogel affords a high surface area of 363.86 $m^2 g^{-1}$, which is a slight decrease in porosity relative to the nonstretched BC aerogel (410.72 $m^2 g^{-1}$) (Figure 5a). The pore-size distribution is further delineated from Figure 5b, indicating the presence of micropores (<2 nm), mesopores (2–50 nm), and macropores (>50 nm) in the BC aerogels.[29] The dominant mesopores in both the BC and aligned BC (ABC) aerogels are clearly seen, whereas the ABC aerogel has a narrower pore-size distribution compared with the BC aerogel. The highly porous and well-aligned structures of organic BC aerogels would facilitate the ion (Ca^{2+}, HPO_4^{2-}, and PO_4^{3-}) transportation and interaction with cellulose nanofibers and eventually the formation of HAP minerals.

The X-ray diffraction (XRD) patterns of NMBC and AMBC composites are given in Figure 5c. In the case of the pure BC aerogel (Figure S4), three broad peaks appear at 14.8, 16.9, and 22.8°. The broadness of the three characteristic peaks corresponds to the typical ($1\bar{1}0$), (110), and (020) planes of cellulose I, respectively.[30] The three peaks assigned to BC become weak but are still observed in NMBC and AMBC composites.[31] The decrease in the intensity of the cellulose peaks in the patterns shows that HAP minerals were the dominating component of the composite. In addition, the mineralized BC aerogel composites displayed mineral diffraction peaks at 22.6, 25.7, 28.1, 31.4, 32.3, 33.6, 39.4, 40.4, 41.8, 43.7, 46.5, and 49.2°, corresponding to the (111), (002), (210), (211), (300), (202), (212), (310), (311), (113), (222), and (213) planes of HAP.[19,31−34] This result clearly indicated that HAP crystals were formed on the organic BC fibril scaffold due to the cycle mineralization treatment.[35] The sharp peaks indicated that the mineralized BC aerogel composites were highly crystalline.[36] To further confirm the chemical structure, the Fourier transform infrared (FTIR) spectroscopy graphs were analyzed (Figure 5d). The FTIR spectrum of the pure BC aerogel is typical, where the absorption band assigned to −OH stretching and bending vibrations was observed at 3200–3500 cm^{-1} (Figure S5).[13]

DOI: 10.1021/acsami.9b15234
ACS Appl. Mater. Interfaces XXXX, XXX, XXX−XXX

Similarities were observed among the NMBC and AMBC composite samples. Whereas the 3200−3500 cm^{-1} peak nearly disappeared in the two spectra of the mineralized BC aerogel composites, the vibrational modes of PO_4^{3-} groups are seen at 1030, 962, 595, and 562 cm^{-1}. In addition, the peak at 869 cm^{-1} occurs due to the stretching mode of the HPO_4^{2-} vibration.[31] These characteristic phosphate peaks verify the presence of HAP minerals.[37]

As confirmed, the hydroxyl groups and calcium and phosphate ions exist in the mineralized BC composites. The formation of the interaction bonds between the BC and HAP stabilizes the composite, which can maintain the mechanical integrity requirements for bone substitution. As indicated in Figure 5e, the hydroxyl groups on the cellulose have a strong negative dipole that chelates free Ca^{2+} cations from the $CaCl_2$ solution. A coordinated bond is formed through the electrostatic interaction between the ion and cellulose. Phosphate ions then form strong ionic bonds with the cellulose-trapped calcium ions to form HAP crystals. The anionic hydroxyl groups concentrate inorganic calcium ions, which proceed to nucleate oriented HAP crystals. The AMBC composite has a uniform distribution of HAP mineral crystals throughout the aligned organic BC nanofibers. In such a way, the organic BC matrix can transfer the stresses to the inorganic HAP mineral component, which helps to bear the mechanical load.[31]

The mechanical properties of the mineralized BC composites were measured experimentally by performing nanoindentations under dry conditions. The nanomechanical test of mineralized BC composites is shown in Figure 6a. A Berkovich diamond tip was used to indent the surface of the NMBC and AMBC samples. The load applied to the tip and the depth of penetration were subsequently measured during the process. Meanwhile, the unloading portion of the load−depth data contains the information on the stiffness of NMBC and AMBC composites, which was related to the contact area. The test included a loading−holding−unloading process. Figure 6b−d shows the representative nanoindentation load−displacement curves and the dependency of the elastic modulus versus the penetration depth of the indenter as well as the hardness versus the displacement on the NMBC and AMBC composites in the dry states. The elastic modulus and hardness values of the NMBC and AMBC composite samples are averaged in Table 1. The NMBC composite shows low values of elastic modulus (3.52 ± 0.97 GPa) and hardness (0.19 ± 0.09 GPa). After stretching, the AMBC composite has an average elastic modulus value (10.91 ± 3.26 GPa) three times greater than the NMBC composite elastic modulus and higher than that of mouse trabecular bone (Figure 6e). The hardness of the AMBC composite sample is 0.37 ± 0.18 GPa, which is smaller than that of human trabecular bone but comparable to that of mouse trabecular bone;[38] however, it is almost three times higher than that of rabbit trabecular bone (Figure 6f).[40] Overall, the AMBC composite possesses a 210% higher elastic modulus and 95% higher hardness compared with the NMBC composite. In addition, the tensile strengths of the BC and ABC films are shown in Figure 6g. The aligned BC film shows a significantly improved tensile strength (210.6 MPa), which is two times larger than that of the nonaligned BC film. In the current study, the dry weight of the mineralized composites and the mass of their respective HAP components are measured based on the weighing method, as shown in Figure 6h. A high mineral content as high as 89.53 wt % of the AMBC composite is achieved, which is just slightly less than that of the NMBC composite, with 91.86 wt % mineral. The mean value of the elastic modulus (10.91 ± 3.26 GPa) in the AMBC composite is higher than the value reported for mineralized collagen films (with a cross-linking density of 82%), and the mean value of hardness (0.37 ± 0.18 GPa) is comparable to that of the previously reported mineralized collagen films (with a cross-linking density of 26%).[8] This significant increase in the modulus and hardness in the AMBC composite is probably due to the highly packed mineralized structure with the HAP minerals in close proximity to the stretched organic BC nanofibers.

Table 1. Elastic Modulus and Hardness Values

samples	elastic modulus (GPa)	hardness (GPa)
NMBC	3.52 ± 0.97	0.19 ± 0.07
AMBC	10.91 ± 1.26	0.37 ± 0.09
human trabecular bone	12.25 ± 1.01	0.68 ± 0.11
mouse trabecular bone	7.42 ± 1.34	0.39 ± 0.16
rabbit trabecular bone	16.60 ± 1.70	0.13 ± 0.04

CONCLUSIONS

Bioinspired by the structure and composition of natural bone, mineralization with the aligned organic BC nanofibers as a template has been studied in this work. We demonstrated that the organic BC aerogel with aligned nanofibers is an ideal template for the ordered mineralization. Because of the unique aligned organic cellulose nanofibers, porous channels, and high specific surface area, the HAP mineral crystals were uniformly distributed throughout the aligned organic BC nanofibers and preferentially distributed along the fibers axes. The AMBC composite exhibits a high elastic modulus and hardness of 10.91 ± 3.26 GPa and 0.37 ± 0.18 GPa, respectively, which are a 210% higher elastic modulus and 95% higher hardness than those of the counterpart NMBC composite. These values are comparable to those of mouse trabecular bone and to the best mineralized organic materials ever reported. The biomimetic mineralization of aligned organic BC aerogel with a high mineral content and excellent mechanical properties inspires a sustainable strategy toward the development of bone substitutes.

EXPERIMENTAL SECTION

Materials. *Acetobacter xylinum* ATCC 23767 was obtained from Guangdong Microbial Culture Center. $CaCl_2{\cdot}2H_2O$ (≥99.0 wt %) and K_2HPO_4 (≥98.0 wt %) were purchased from Sigma. All other chemicals were analytical grade and used as received without further purification. All aqueous solutions were prepared with ultrapure water (>18.2 MΩ cm) from a Milli-Q Plus system (Millipore). All glassware used in the following procedures were cleaned with ethanol and rinsed thoroughly with ultrapure water prior to use.

Fabrication of Bacterial Cellulose Hydrogel. The BC hydrogel with a fiber content of 0.5% (m/m) was generated by an *Acetobacter xylinum* fermentation process.[41] The *Acetobacter xylinum* (ATCC 23767) was inoculated into the liquid production media at 30 °C in a bulk container.[42] The inoculum contained 20.0 g L^{-1} glucose, 5.0 g L^{-1} bacto-peptone, 5.0 g L^{-1} yeast extract, 15.0 g L^{-1} D-mannitol, 2.5 g L^{-1} Na_2HPO_4, 2.0 g L^{-1} citric acid, and 5.0 g L^{-1} anhydrous ethanol. The liquid media were subjected to high-pressure sterilization (121 °C for 20 min) before cultivation.[9] A pellicle of BC hydrogel was obtained after static culture fermentation at 30 °C for 7 days. The as-prepared BC was soaked in 0.5 mol L^{-1} NaOH solution and then rinsed with deionized water until the residues were neutralized.

DOI: 10.1021/acsami.9b15234
ACS Appl. Mater. Interfaces XXXX, XXX, XXX−XXX

Stretching of Bacterial Cellulose Hydrogel. A piece of purified BC pellicle was cut into a rectangular shape of size 30 mm × 20 mm × 110 mm. The strip of BC pellicle was mounted between two custom-made grips, where one grip was fixed and the other could be moved up and down. Then, the pellicle was wet-drawn at a constant speed until the stretch of the sample reached 20%.[22] For comparison purposes, the original BC hydrogel (nonstretched) was prepared in the same manner by processing from a piece of the same BC pellicle.

Fabrication of BC Aerogel. The stretched and nonstretched BC hydrogel samples were first frozen by liquid nitrogen and then were freeze-dried for 72 h to obtain the aligned BC and original BC aerogel.[43]

Mineralization of BC. For the synthesis of mineralized BC aerogel nanocomposites, inorganic minerals were formed in the BC aerogel by performing alternating impregnation cycles with $CaCl_2$ and K_2HPO_4 solutions.[31] An impregnation cycle is defined as suspending the BC aerogel in 250 mmol/L $CaCl_2$ under agitation in a shaker for 24 h, including sonication under ambient conditions with a high-density ultrasonic probe for 30 min (10 min every time) to allow for in-depth diffusion into the porous structure, and then degassing to ensure full infiltration. The BC was then briefly rinsed in deionized water. Then, the sample was transferred to 150 mmol/L K_2HPO_4 under agitation for another 24 h, including sonication under ambient condition with a high-density ultrasonic probe for another 30 min (the same procedure as above). At last, the product was washed with deionized water. The NMBC and AMBC composites were synthesized with four impregnation cycles.

Calculation of the Weight of Mineralized BC Composites. First, the BC and ABC aerogel were weighed by the electronic balance. NMBC and AMBC composites were dried in an oven at 80 °C for 48 h before their mass was weighed. Thus the HAP mineral components in NMBC and AMBC composites were obtained by subtracting the weight of BC from the NMBC composite and the weight of ABC from the AMBC composite, respectively.

Scanning Electron Microscopy. SEM (S3700 Hitachi, Japan) was used to examine the morphology of the BC films, BC aerogel, and mineralized BC composite. The fixed samples were coated with a layer of ∼30 Å thick gold. The accelerating voltage was 10 kV, and the working distance was 11 mm. For the elemental analysis of mineralized samples, an EDX spectroscopy analysis was performed during the SEM examination.

Fourier Transform Infrared Spectroscopy. The mineralized BC composites were deposited onto the KBr slice, and the FTIR spectra of the composites were recorded using a Nicolet FTIR 5700 spectrophotometer (Bruker, Germany) in transmission mode over the range of 500−4000 cm^{-1} with a 4 cm^{-1} resolution at 25 °C.

X-ray Diffraction. XRD tests were conducted on an X-ray diffractometer (Ultima IV, Japan) using Cu Kα radiation at 40 kV and 30 mA. The scan is from 2θ of 20 to 50° at a step size of 0.05°.

Brunauer−Emmett−Teller Test. The surface area of the BC aerogel was studied on a TriStar II 3020 surface area analyzer (Micromeritics Instruments) by using N_2 gas adsorption at 77 K. The surface area was calculated according to the BET analysis method. The pore-size distribution was calculated from the desorption branch of the isotherm curve according to the Barrett−Joyner−Halenda method.

Tensile Test. Tensile mechanical properties of dried BC films (5 mm width × 25 mm length × 1 mm thickness) were assessed by applying incremental tensional forces with an Instron model 5567 machine with crosshead speed control of 100 mm/min at room temperature (RT).

Nanoindentation. The mechanical properties of the BC aerogel before and after mineralization were examined using an MTS Nanoindenter XP apparatus equipped with a Berkovich tip at RT. TestWorks 4 software was used to analyze the elastic modulus and hardness. The dried NMBC and AMBC samples were embedded in epoxy resin, sectioned to reveal an indentation surface, and polished with polishing papers (SiC, 600, 800, and 1200) and alumina slurries (1, 0.3, and 0.05 μm, respectively). A total of 20 indents were performed on the sample surface. The maximum indentation depth was set at 2000 nm. The Oliver−Pharr data analysis method was used to analyze the elastic modulus and hardness at the depth of 2000 nm.

Statistical Analysis. The analysis of the statistically significant differences of mechanical properties among groups was performed with one-way ANOVA tables. The level of statistical significance was set at $p < 0.05$.[8,44]

■ ASSOCIATED CONTENT

Supporting Information

The Supporting Information is available free of charge on the ACS Publications website at DOI: 10.1021/acsami.9b15234.

Photographs of BC hydrogel in the twisted, stretched, bent, and folded states; photograph of the AMBC composite; SEM image of the cross-section of the NMBC composite; XRD patterns of BC aerogel; and FTIR spectra of BC aerogel (PDF)

■ AUTHOR INFORMATION

Corresponding Authors

*E-mail: h.zhu@northeastern.edu (H.Z.).
*E-mail: apari003@umn.edu (C.A.).

ORCID

Zhou Ye: 0000-0003-4220-0919
Conrado Aparicio: 0000-0003-2969-6067
Hongli Zhu: 0000-0003-1733-4333

Notes

The authors declare no competing financial interest.

■ ACKNOWLEDGMENTS

H.Z. acknowledges the financial support from NSF ECC-SEPMD: 1933051. We thank the Kostas Research Institute at Northeastern University for the use of their facilities and Dr. David Nedrelow for his technical support during nano-indentation tests.

■ REFERENCES

(1) Gao, H.; Ji, B.; Jäger, I. L.; Arzt, E.; Fratzl, P. Materials become insensitive to flaws at nanoscale: lessons from nature. *Proc. Natl. Acad. Sci. U. S. A.* **2003**, *100* (10), 5597−5600.

(2) Ling, S.; Jin, K.; Qin, Z.; Li, C.; Zheng, K.; Zhao, Y.; Wang, Q.; Kaplan, D. L.; Buehler, M. J. Combining In Silico Design and Biomimetic Assembly: A New Approach for Developing High-Performance Dynamic Responsive Bio-Nanomaterials. *Adv. Mater.* **2018**, *30* (43), 1802306.

(3) Chen, S.-M.; Gao, H.-L.; Sun, X.-H.; Ma, Z.-Y.; Ma, T.; Xia, J.; Zhu, Y.-B.; Zhao, R.; Yao, H.-B.; Wu, H.-A.; Yu, S.-H. Superior Biomimetic Nacreous Bulk Nanocomposites by a Multiscale Soft-Rigid Dual-Network Interfacial Design Strategy. *Matter* **2019**, *1* (2), 412−427.

(4) Olszta, M. J.; Cheng, X.; Jee, S. S.; Kumar, R.; Kim, Y.-Y.; Kaufman, M. J.; Douglas, E. P.; Gower, L. B. Bone structure and formation: a new perspective. *Mater. Sci. Eng., R* **2007**, *58* (3−5), 77−116.

(5) Sarkar, C.; Kumari, P.; Anuvrat, K.; Sahu, S. K.; Chakraborty, J.; Garai, S. Synthesis and characterization of mechanically strong carboxymethyl cellulose−gelatin−hydroxyapatite nanocomposite for load-bearing orthopedic application. *J. Mater. Sci.* **2018**, *53* (1), 230−246.

(6) Maas, M.; Guo, P.; Keeney, M.; Yang, F.; Hsu, T. M.; Fuller, G. G.; Martin, C. R.; Zare, R. N. Preparation of mineralized nanofibers: collagen fibrils containing calcium phosphate. *Nano Lett.* **2011**, *11* (3), 1383−1388.

(7) Osathanon, T.; Linnes, M. L.; Rajachar, R. M.; Ratner, B. D.; Somerman, M. J.; Giachelli, C. M. Microporous nanofibrous fibrin-

DOI: 10.1021/acsami.9b15234
ACS Appl. Mater. Interfaces XXXX, XXX, XXX−XXX

based scaffolds for bone tissue engineering. *Biomaterials* **2008**, *29* (30), 4091−4099.
(8) Li, Y.; Thula, T. T.; Jee, S.; Perkins, S. L.; Aparicio, C.; Douglas, E. P.; Gower, L. B. Biomimetic mineralization of woven bone-like nanocomposites: role of collagen cross-links. *Biomacromolecules* **2012**, *13* (1), 49−59.
(9) Cheng, Z.; Yang, R.; Liu, X.; Liu, X.; Chen, H. Green synthesis of bacterial cellulose via acetic acid pre-hydrolysis liquor of agricultural corn stalk used as carbon source. *Bioresour. Technol.* **2017**, *234*, 8−14.
(10) Li, H.; Cheng, Z.; Zhang, Q.; Natan, A.; Yang, Y.; Cao, D.; Zhu, H. Bacterial-Derived, Compressible, and Hierarchical Porous Carbon for High-Performance Potassium-Ion Batteries. *Nano Lett.* **2018**, *18* (11), 7407−7413.
(11) Hu, S.-Q.; Gao, Y.-G.; Tajima, K.; Sunagawa, N.; Zhou, Y.; Kawano, S.; Fujiwara, T.; Yoda, T.; Shimura, D.; Satoh, Y.; et al. Structure of bacterial cellulose synthase subunit D octamer with four inner passageways. *Proc. Natl. Acad. Sci. U. S. A.* **2010**, *107* (42), 17957−17961.
(12) Fernandes, S. C.; Sadocco, P.; Alonso-Varona, A.; Palomares, T.; Eceiza, A.; Silvestre, A. J.; Mondragon, I. a.; Freire, C. S. Bioinspired antimicrobial and biocompatible bacterial cellulose membranes obtained by surface functionalization with aminoalkyl groups. *ACS Appl. Mater. Interfaces* **2013**, *5* (8), 3290−3297.
(13) Wan, Y.; Huang, Y.; Yuan, C.; Raman, S.; Zhu, Y.; Jiang, H.; He, F.; Gao, C. Biomimetic synthesis of hydroxyapatite/bacterial cellulose nanocomposites for biomedical applications. *Mater. Sci. Eng., C* **2007**, *27* (4), 855−864.
(14) Hutmacher, D. W. Scaffolds in Tissue Engineering Bone and Cartilage. In *The Biomaterials: Silver Jubilee Compendium*; Elsevier: 2006; pp 175−189.
(15) Lin, N.; Dufresne, A. Nanocellulose in biomedicine: Current status and future prospect. *Eur. Polym. J.* **2014**, *59*, 302−325.
(16) Liu, Y.; Li, N.; Qi, Y. p.; Dai, L.; Bryan, T. E.; Mao, J.; Pashley, D. H.; Tay, F. R. Intrafibrillar collagen mineralization produced by biomimetic hierarchical nanoapatite assembly. *Adv. Mater.* **2011**, *23* (8), 975−980.
(17) Qi, Y.; Cheng, Z.; Ye, Z.; Zhu, H.; Aparicio, C. Bio-Inspired Mineralization with Hydroxyapatite and Hierarchical Natural Aligned Nanofibrillar Cellulose. *ACS Appl. Mater. Interfaces* **2019**, *11*, 27598.
(18) Siró, I.; Plackett, D. Microfibrillated cellulose and new nanocomposite materials: a review. *Cellulose* **2010**, *17* (3), 459−494.
(19) Rodríguez, K.; Renneckar, S.; Gatenholm, P. Biomimetic calcium phosphate crystal mineralization on electrospun cellulose-based scaffolds. *ACS Appl. Mater. Interfaces* **2011**, *3* (3), 681−689.
(20) Petrauskaite, O.; Gomes, P. d. S.; Fernandes, M. H.; Juodzbalys, G.; Stumbras, A.; Maminskas, J.; Liesiene, J.; Cicciù, M. Biomimetic mineralization on a macroporous cellulose-based matrix for bone regeneration. *BioMed Res. Int.* **2013**, *2013*, 1.
(21) Wang, S.; Jiang, F.; Xu, X.; Kuang, Y.; Fu, K.; Hitz, E.; Hu, L. Super-Strong, Super-Stiff Macrofibers with Aligned, Long Bacterial Cellulose Nanofibers. *Adv. Mater.* **2017**, *29* (35), 1702498.
(22) Wang, S.; Li, T.; Chen, C.; Kong, W.; Zhu, S.; Dai, J.; Diaz, A. J.; Hitz, E.; Solares, S. D.; Li, T.; et al. Transparent, anisotropic biofilm with aligned bacterial cellulose nanofibers. *Adv. Funct. Mater.* **2018**, *28*, 1707491.
(23) Luo, H.; Xiong, G.; Zhang, C.; Li, D.; Zhu, Y.; Guo, R.; Wan, Y. Surface controlled calcium phosphate formation on three-dimensional bacterial cellulose-based nanofibers. *Mater. Sci. Eng., C* **2015**, *49*, 526−533.
(24) Weiner, S.; Traub, W. Bone structure: from angstroms to microns. *FASEB J.* **1992**, *6* (3), 879−885.
(25) Weiner, S.; Wagner, H. D. The material bone: structure-mechanical function relations. *Annu. Rev. Mater. Sci.* **1998**, *28* (1), 271−298.
(26) Wang, X.; Cui, F.; Ge, J.; Wang, Y. Hierarchical structural comparisons of bones from wild-type and liliputdtc232 gene-mutated Zebrafish. *J. Struct. Biol.* **2004**, *145* (3), 236−245.
(27) Palmer, L. C.; Newcomb, C. J.; Kaltz, S. R.; Spoerke, E. D.; Stupp, S. I. Biomimetic systems for hydroxyapatite mineralization inspired by bone and enamel. *Chem. Rev.* **2008**, *108* (11), 4754−4783.
(28) Dorozhkin, S. V.; Epple, M. Biological and medical significance of calcium phosphates. *Angew. Chem., Int. Ed.* **2002**, *41* (17), 3130−3146.
(29) Xu, X.; Zhou, J.; Nagaraju, D. H.; Jiang, L.; Marinov, V. R.; Lubineau, G.; Alshareef, H. N.; Oh, M. Flexible, Highly Graphitized Carbon Aerogels Based on Bacterial Cellulose/Lignin: Catalyst-Free Synthesis and its Application in Energy Storage Devices. *Adv. Funct. Mater.* **2015**, *25* (21), 3193−3202.
(30) Hu, Y.; Abidi, N. Distinct chiral nematic self-assembling behavior caused by different size-unified cellulose nanocrystals via a multistage separation. *Langmuir* **2016**, *32* (38), 9863−9872.
(31) Hutchens, S. A.; Benson, R. S.; Evans, B. R.; O'Neill, H. M.; Rawn, C. J. Biomimetic synthesis of calcium-deficient hydroxyapatite in a natural hydrogel. *Biomaterials* **2006**, *27* (26), 4661−4670.
(32) Siddharthan, A.; Seshadri, S. K.; Kumar, T. S. S. Microwave accelerated synthesis of nanosized calcium deficient hydroxyapatite. *J. Mater. Sci.: Mater. Med.* **2004**, *15* (12), 1279−1284.
(33) Fu, L.-H.; Qi, C.; Liu, Y.-J.; Cao, W.-T.; Ma, M.-G. Sonochemical synthesis of cellulose/hydroxyapatite nanocomposites and their application in protein adsorption. *Sci. Rep.* **2018**, *8* (1), 8292.
(34) Sarkar, C.; Kumari, P.; Anuvrat, K.; Sahu, S. K.; Chakraborty, J.; Garai, S. Synthesis and characterization of mechanically strong carboxymethyl cellulose−gelatin−hydroxyapatite nanocomposite for load-bearing orthopedic application. *J. Mater. Sci.* **2018**, *53* (1), 230−246.
(35) Koutsopoulos, S. Synthesis and characterization of hydroxyapatite crystals: a review study on the analytical methods. *J. Biomed. Mater. Res.* **2002**, *62* (4), 600−612.
(36) Klemm, D.; Heublein, B.; Fink, H. P.; Bohn, A. Cellulose: fascinating biopolymer and sustainable raw material. *Angew. Chem., Int. Ed.* **2005**, *44* (22), 3358−3393.
(37) Sato, K.; Kogure, T.; Kumagai, Y.; Tanaka, J. Crystal orientation of hydroxyapatite induced by ordered carboxyl groups. *J. Colloid Interface Sci.* **2001**, *240* (1), 133−138.
(38) Norman, J.; Shapter, J. G.; Short, K.; Smith, L. J.; Fazzalari, N. L. Micromechanical properties of human trabecular bone: a hierarchical investigation using nanoindentation. *J. Biomed. Mater. Res., Part A* **2008**, *87A* (1), 196−202.
(39) Kavukcuoglu, N. B.; Patterson-Buckendahl, P.; Mann, A. B. Effect of osteocalcin deficiency on the nanomechanics and chemistry of mouse bones. *Journal of the Mechanical Behavior of Biomedical Materials* **2009**, *2* (4), 348−354.
(40) Soares, P. B. F.; Nunes, S. A.; Franco, S. D.; Pires, R. R.; Zanetta-Barbosa, D.; Soares, C. J. Measurement of elastic modulus and Vickers hardness of surround bone implant using dynamic microindentation-parameters definition. *Brazilian dental journal* **2014**, *25* (5), 385−390.
(41) Li, H.; Cheng, Z.; Zhang, Q.; Natan, A.; Yang, Y.; Cao, D.; Zhu, H. Bacterial-Derived, Compressible and Hierarchical Porous Carbon for High Performance Potassium-ion Batteries. *Nano Lett.* **2018**, *18*, 7407.
(42) Cheng, Z.; Yang, R.; Liu, X. Production of bacterial cellulose by Acetobacter xylinum through utilizing acetic acid hydrolysate of bagasse as low-cost carbon source. *BioResources* **2016**, *12* (1), 1190−1200.
(43) Chen, L.-F.; Huang, Z.-H.; Liang, H.-W.; Yao, W.-T.; Yu, Z.-Y.; Yu, S.-H. Flexible all-solid-state high-power supercapacitor fabricated with nitrogen-doped carbon nanofiber electrode material derived from bacterial cellulose. *Energy Environ. Sci.* **2013**, *6* (11), 3331−3338.
(44) Leong, P.; Morgan, E. Measurement of fracture callus material properties via nanoindentation. *Acta Biomater.* **2008**, *4* (5), 1569−1575.

DOI: 10.1021/acsami.9b15234
ACS Appl. Mater. Interfaces XXXX, XXX, XXX−XXX